Supporting Material

General Equations

Sarcolemmal Membrane Potential

Sarcolemmal membrane potential. In this study, two forms of electrical stimuli are utilized to trigger LCC opening and CICR, “voltage clamp” and “current clamp”. The “voltage clamp” protocol forces a step change in sarcolemmal membrane potential while a small inward current, I_{app}, is applied in the “current clamp” protocol to elicit an action potential. The sarcolemmal membrane potential during ”current-clamp” mode is governed by

$$-C_m \frac{dV}{dt} = \left(I_{lcc}^T + I_{lcc,nj} + I_{ncx} + I_{nak} + I_{pmca} + I_{k1} + I_{kss} + I_{ktof} + I_{ktos} + I_b + I_{app} \right) \tag{S1}$$

where C_m is the membrane capacitance, Ina is the fast sodium (Na^+) current, I_{k1} is the inwardly rectifying K^+ current, I_{kss} is the non-inactivating steady-state voltage-activated K^+ current, I_{ktof} is the rapidly inactivating transient outward potassium K^+ current, I_{ktos} is the slowly inactivating transient outward potassium K^+ current, I_{nak} is the Na^+/K^+ pump current, I_{ncx} is the Na^+/Ca^{2+} exchanger (NCX) current, I_{pmca} is the plasma membrane Ca^{2+}-ATPase (PMCA) current, I_{lcc}^T is the whole-cell, junctional L-type Ca^{2+} (LCC) current, $I_{lcc,nj}$ is the whole-cell, non-junctional L-type Ca^{2+} current, and I_{app} is the stimulus current applied during cell pacing. I_b, represents the combined background Ca^{2+}, Na^+, and K^+ currents. The formulation of K^+ currents can be found below and are primarily based on the currents from the mouse action potential model by Bondarenko and co-workers [1]. The fast Na^+ current is adapted from [2] and is also outlined below.

Concentration Balance Equations

The Monte Carlo model presented here consists of 2N + 4 (N = 20,000) ODEs representing the time-evolution of various intracellular ion concentrations (i.e., $[Ca^{2+}]_i, [K^+]_i, [Na^+]_i$, etc). Consistent with Fig. 1, the concentration balance equations are

$$\frac{[Ca^{2+}]_i}{dt} = \beta_{myo} \left(J_{efflux}^T - J_{ncx} - J_{serca} + J_{bca} - J_{pmca} + J_{ryr,nj} + J_{lcc,nj} - J_{buffer} - J_{CaF} \right) \tag{S2}$$

$$\frac{[Ca^{2+}]_{nsr}}{dt} = \frac{\beta_{nsr}}{\lambda_{nsr}} \left(J_{serca} - J_{refill}^T - J_{ryr,nj} \right) \tag{S3}$$

$$\frac{[Ca^{2+}]_{jsr}^n}{dt} = \frac{\beta_{jsr}^n}{\lambda_{jsr}} \left(J_{refill}^T - J_{ryr}^n \right) \tag{S4}$$

$$\frac{[Ca^{2+}]_{ds}^n}{dt} = \frac{\beta_{ds}^n}{\lambda_{ds}} \left(J_{lcc}^n + J_{ryr}^n - J_{efflux} \right) \tag{S5}$$

$$\frac{[Na^+]_i}{dt} = \frac{A_m}{FV_{myo}} \left(I_{na} + I_{bna} + 3I_{ncx} - 3I_{nak} \right) \tag{S6}$$

$$\frac{[K^+]_i}{dt} = \frac{A_m}{FV_{myo}} \left(I_{k1} + I_{kss} + I_{ktof} + I_{ktos} + I_{bk} - 2I_{nak} \right) \tag{S7}$$

where $1 \leq n \leq N$, λ_{nsr}, λ_{jsr}, and λ_{ds} are volume fractions (see Table S1), β_{jsr} and β_{nsr} are constant fraction buffering constants (see Table S7), and β_{myo} is the dynamic buffering fraction for the bulk myoplasm (see SI Eq. S45). See the SI for ODEs which govern gating variables for non-stochastic channels (i.e., K^+ and Na^+ channels). Note that all ”whole-cell” flux terms (e.g., J_{ncx}, J_{ryr}^T, etc.) have units of μM s^{-1} (scaled to a liter of cytosol) and are defined in the SI. All currents (e.g., I_{ncx}, I_{lcc}^T, etc.) have units of pA/pF and are also defined in the SI. Note that the $[Ca^{2+}]$ in each subspace ($[Ca^{2+}]_{ds}^n$) is assumed to be in rapid equilibrium with the $[Ca^{2+}]$ in the respective JSR ($[Ca^{2+}]_{jsr}^n$) and $[Ca^{2+}]_i$(see [8, 7, 6]) allowing Eq. S5 to be reduced to an algebraic expression of the form,

$$[Ca^{2+}]_{ds} = \frac{N_{L,O}^n J_{lcc}^0 + v_{efflux}[Ca^{2+}]_i + N_{R,O}^n v_{ryr}[Ca^{2+}]_{jsr}^n}{N_{R,O}^n v_{ryr} + v_{efflux} - N_{L,O}^n J_{lcc}^0} \tag{S8}$$

where $N^{n}_{L,O}$ and $N^{n}_{R,O}$ represent the number of open LCCs and RyR2s (respectively) at the n^{th} CRU. The terms J^{0}_{lcc} and J^{1}_{lcc} are functions of membrane potential (V) and are defined by $J_{lcc} = J^{0}_{lcc} + [Ca^{2+}]^{n}_{ds} J^{1}_{lcc}$ with J_{lcc} as in Eq. S25. This is significant in that reduces the number of ODEs (for intracellular ion concentrations) from 2N+4 to N+4, a nearly 2 fold reduction in computational demand. Each ODE was solved using the first-order Euler method with a variable time-step designed to ensure stability.

Gating variables for membrane currents.

The gating variables for Na^{+} membrane currents are governed by the following ODEs,

$$\frac{dm_{na}}{dt} = \alpha_{m,na}(1 - m_{na}) - \beta_{m,na} m_{na} \tag{S9}$$

$$\frac{dh_{na}}{dt} = \alpha_{h,na}(1 - h_{na}) - \beta_{h,na} h_{na} \tag{S10}$$

$$\frac{dj_{na}}{dt} = \alpha_{j,na}(1 - j_{na}) - \beta_{j,na} j_{na} \tag{S11}$$

where

$$\alpha_{m} = \frac{320(V + 47.13)}{1 - e^{-0.1(V+47.13)}}$$

$$\beta_{m} = 80e^{-V/11}$$

$$\alpha_{h} = 135 * e^{(V+80)/-6.8}$$

$$\beta_{h} = \frac{7500}{1 + e^{-0.1*(V+11)}}$$

$$\alpha_{j} = \frac{175e^{(V+100)/-23}}{1 + e^{0.15*(V+79)}}$$

$$\beta_{j} = \frac{300}{1 + e^{-0.1*(V+32)}}$$

The gating variables for K^{+} membrane currents are governed by the following ODEs,

$$\frac{da_{ktof}}{dt} = (1 - a_{ktof})\,\alpha_{a,ktof} - a_{ktof}\beta_{i,ktof} \tag{S12}$$

$$\frac{di_{ktof}}{dt} = (1 - i_{ktof})\alpha_{i,ktof} - i_{ktof}\beta_{i,ktof} \tag{S13}$$

$$\frac{da_{ktos}}{dt} = \frac{a^{ss}_{ktos} - a_{ktos}}{\tau_{a,ktos}} \tag{S14}$$

$$\frac{di_{ktos}}{dt} = \frac{i^{ss}_{ktos} - i_{ktos}}{\tau_{i,ktos}} \tag{S15}$$

$$\frac{da_{kss}}{dt} = \frac{a^{ss}_{kss} - a_{kss}}{\tau_{kss}} \tag{S16}$$

(S17)

where

$$
\begin{aligned}
\alpha_{a,ktof} &= 180.64e^{0.03577(V+30)} \\
\beta_{a,ktof} &= 395.6e^{-0.06237*(V+30)} \\
\alpha_{i,ktof} &= \frac{0.152e^{-(V+13.5)/7}}{0.067083e^{-(V+33.5)/7}+1} \\
\beta_{i,ktof} &= \frac{0.95e^{(V+33.5)/7}}{0.051335e^{(V+33.5)/7}+1} \\
a^{ss}_{ktos} &= (1/(1+e^{-(V+22.5)/7.7})) \\
\tau_{a,ktos} &= 0.493\times10^{-3}e^{-0.0629V}+2.058\times10^{-3}) \\
i^{ss}_{ktos} &= (1/(1+e^{(V+45.2)/5.7})) \\
\tau_{i,ktos} &= (0.27+1.05/(1+e^{(V+45.2)/5.7}) \\
a^{ss}_{kss} &= (1/(1+e^{-(V+22.5)/7.7})) \\
\tau_{kss} &= 0.393\times10^{-3}e^{-0.0862V}+0.13\times10^{-3}
\end{aligned}
$$

K^+ membrane currents

The fast inactivating K^+ current is given by,

$$I_{ktof} = a_{ktof}i_{ktof}g_{ktof}(V-E_k) \tag{S18}$$

where a_{ktof} and i_{ktof} are the activation and inactivation gates, respectively, g_{ktof} is the conductance, and E_k is the Nernst reversal potential for K^+ (see Eq. S53). The slowly inactivating K^+ current is given by,

$$I_{ktos} = a_{ktos}i_{ktos}g_{ktos}(V-E_k) \tag{S19}$$

where a_{ktos} and i_{ktos} are the activation and inactivation gates, respectively, g_{ktos} is the conductance, and E_k is the Nernst reversal potential for K^+ (see Eq. S53). The steady-state (non-inactivating) K^+ current is given by,

$$I_{kss} = a_{kss}g_{kss}(V-E_k) \tag{S20}$$

where a_{kss} is the activation gate, g_{ktof} is the conductance, and E_k is the Nernst reversal potential for K^+ (see Eq. S53). The always on K^+ current is given by,

$$I_{k1} = g_{k1}(V-E_k) \tag{S21}$$

where g_{k1} is the conductance and E_k is the Nernst reversal potential for K^+ (see Eq. S53). The background K^+ current is given by,

$$I_{bk} = g_{bk}(V-E_k) \tag{S22}$$

where g_{bk} is the conductance and E_k is the Nernst reversal potential for K^+ (see Eq. S53).

Na^+ membrane current

The fast Na^+ current is given by,

$$I_{na} = m_{na}h_{na}j_{na}g_{na}(V-E_{na}) \tag{S23}$$

where m_{na}, h_{na}, and j_{na} are the gating variables (see Eqs. S9–S11, respectively), g_{na} is the conductance, and E_{na} is the Nernst reversal potential for Na^+ (see Eq. S52). The background Na^+ current is given by,

$$I_{bna} = g_{bna}(V-E_{na}) \tag{S24}$$

where g_{na} is the conductance and E_{na} is the Nernst reversal potential for Na^+ (see Eq. S52).

Ca^{2+} Fluxes

L-type Ca^{2+} Channel Flux

The L-type Ca^{2+} flux into each of the N diadic spaces (J^n_{lcc}) is given by

$$J^n_{lcc} = -\frac{I^n_{lcc}}{zFV_{myo}} \tag{S25}$$

where z is the valency for Ca^{2+}, F is Faraday's constant, and V_{myo} is the volume of the myoplasm in μL. Accordingly, the inward Ca^{2+} current is given by

$$I^n_{lcc} = N^n_{L,O} P_{lcc} \left(\frac{zFV}{V_\theta}\right) \left(\frac{[Ca^{2+}]^n_{ds} e^{V/V_\theta} - 0.341[Ca^{2+}]_o}{e^{V/V_\theta} - 1}\right) \tag{S26}$$

where $V_\theta = RT/zF$, P_{lcc} is the single channel permeability of the L-type Ca^{2+} channels, and $N^n_{L,O}$ is the number of open L-type Ca^{2+} channels associated with the n^{th} CRU. Therefore, the whole-cell, junctional LCC current is given by,

$$I^T_{lcc} = \sum_{n=1}^{N} I^n_{lcc} \tag{S27}$$

Non-junctional L-type Ca^{2+} Channel Flux

The non-junctional L-type Ca^{2+} flux into the bulk myoplasm ($J_{lcc,nj}$ in Eq. 3) is given by

$$J_{lcc,nj} = -\frac{I_{lcc,nj}}{zFV_{myo}} \tag{S28}$$

The inward Ca^{2+} current is given by

$$I_{lcc,nj} = \pi^o_L P_{lcc,nj} \left(\frac{zFV}{V_\theta}\right) \left(\frac{[Ca^{2+}]_i e^{V/V_\theta} - 0.341[Ca^{2+}]_o}{e^{V/V_\theta} - 1}\right) \tag{S29}$$

where π^o_L is the probability of finding a non-junctional LCC in the open state.

The probability of finding an LCC in each of its 7 states is governed by,

$$\frac{d\pi_L}{dt} = \pi_L Q \tag{S30}$$

where π_L is a 1 X M_L row vector of state probabilities, Q is the M_L X M_L infinitesimal generator matrix for the discrete-state, continuous-time Markov chain used to describe the stochastic gating of the LCC (see Fig. 1 B), and M_L is the number of states in the LCC model (M_L=7) . For the seven-state LCC shown in Fig. 1 B, π^o_L is seventh entry in π_L.

L-type Ca^{2+} Channel Transitions

$$v_a = \frac{e^{(V-V_{\theta,1})/V_{\sigma,1}}}{1 + e^{V-V_{\theta,1}/V_{\sigma,1}}} \tag{S31}$$

$$v_i = 1 - \frac{1}{1 + e^{(V+V_{\theta,2})/V_{\sigma,2}}} + \frac{0.27}{1 + e^{(V_{\theta,3}-V)/V_{\sigma,3}}} \tag{S32}$$

$$v_d = 1 + X_{vd} * \left(1 - \frac{e^{(V-V_{theta,4})/V_{sigma,4}}}{1 + e^{(V-V_{theta,4})/V_{sigma,4}}}\right) \tag{S33}$$

$$c = ([Ca^{2+}]^n_{ds})^{\eta_L} \tag{S34}$$

Sarcoplasmic/Endoplasmic Reticulum Ca^{2+}-ATPase

The sarcoplasmic/endoplasmic reticulum Ca^{2+}-ATPase (SERCA) consumes ATP to pump Ca^{2+} into the SR from the myoplasm. Tran and co-workers [5] developed a thermodynamically realistic formulation of the SERCA pump along with a simplified "two-state" formulation that is implemented here. The SERCA pump flux takes the form,

$$J_{serca} = 2v_{cycle}A_p \tag{S35}$$

where A_p is the concentration of SERCA molecules (μM) and v_{cycle} is the cycling rate (s^{-1}) per pump molecule (see [5])

Na^+-Ca^{2+} Exchanger

The main pathway by which Ca^{2+} is extruded from the myocyte is the Na^+-Ca^{2+} exchanger (NCX) which can be described as

$$J_{ncx} = \frac{-A_m I_{ncx}}{FV_{myo}} \tag{S36}$$

$$I_{ncx} = F_A I_{ncx}^{max} \frac{[Na^+]_i^3[Ca^{2+}]_o e^{(\eta_{ncx}FV/RT)} - [Na^+]_o^3[Ca^{2+}]_i e^{(\eta_{ncx}-1)FV/RT}}{\left((K_{ncx,na})^3 + [Na^+]_o^3\right)\left(K_{ncx,ca} + [Ca^{2+}]_o\right)\left(1 + k_{ncx}^{sat} e^{(\eta_{ncx}-1)FV/RT}\right)} \tag{S37}$$

where

$$F_A = \left(\frac{[Ca^{2+}]_i^2}{K_{ma,ncx}^2 + [Ca^{2+}]_i^2}\right)$$

and I_{ncx}^{max} is the maximal NCX current, $[Ca^{2+}]_o$ is the extracellular $[Ca^{2+}]$, and $[Na^+]_i$ and $[Na^+]_o$ are the intracellular and extracellular $[Na^+]$, respectively. All other parameters are given in Table S9.

Plasma Membrane Ca^{2+}-ATPase

In addition to NCX the sarcolemma extrudes Ca^{2+} from the cell via a plasma membrane Ca^{2+}-ATPase flux (PMCA) of the form

$$I_{pmca} = I_{pmca}^{max}\left(\frac{[Ca^{2+}]_i^2}{K_{pmca}^2 + [Ca^{2+}]_i^2}\right) \tag{S38}$$

where I_{pmca}^{max} is the maximal PMCA current.

Na^+/K^+ Pump

The Na^+/K^+ pump (NAK) drives Na^+ out of the cell and K^+ into the cell and to maintain Na^+ and K^+ homeostasis. The NAK membrane current is given by,

$$\begin{aligned} I_{nak} &= I_{nak}^{max} f_{nak} \frac{1}{1 + (K_{m,nai}/[Na^+]_i)^{1.5}} \frac{[K^+]_o}{[K^+]_o + K_{m,ko}} \\ f_{nak} &= \frac{1}{1 + 0.1245e^{-0.1VF/RT} + 0.0365\sigma_{nak}e^{-VF/RT}} \\ \sigma_{nak} &= \frac{1}{7}\left(e^{[Na^+]_o/67,300} - 1\right) \end{aligned} \tag{S39}$$

where I_{nak}^{max} is the maximal NAK current.

Sarcolemmal Background Ca^{2+} Leak

The sarcolemma includes a constant background Ca^{2+} influx which balances J_{pmca} and J_{ncx} given by

$$J_{bca} = -\frac{A_m I_{bca}}{zFV_{myo}} \tag{S40}$$

where z is the valency for Ca^{2+}, $I_{bca} = g_{bca}(V - E_{ca})$, g_{bca} is the maximal conductance, and E_{ca} is the reversal potential for Ca^{2+}(see Eq. S51)

Total JSR refill and dyadic subspace efflux terms

The total refill flux from the NSR to each JSR compartment includes the contribution from each CRU and is given by

$$J^T_{refill} = \sum_{n=1}^{N} J^n_{refill} = \sum_{n=1}^{N} \frac{v^T_{refill}}{N}([Ca^{2+}]_{nsr} - [Ca^{2+}]^n_{jsr}). \tag{S41}$$

and similarly, the total flux out of the N dyadic subspaces into the bulk myoplasm is given by

$$J^T_{efflux} = \sum_{n=1}^{N} J^n_{efflux} = \sum_{n=1}^{N} \frac{v^T_{efflux}}{N}([Ca^{2+}]^n_{ds} - [Ca^{2+}]_i). \tag{S42}$$

Junctional RyR2 Ca^{2+} Release

The Ca^{2+} flux through junctional RyR2s is

$$J^n_{ryr} = N^n_{R,O} v_{ryr,nj}([Ca^{2+}]^n_{jsr} - [Ca^{2+}]^n_{ds}). \tag{S43}$$

where $v_{ryr,nj}$ is the non-junctional RyR junctional release rate in s^{-1}. Therefore, the whole-cell, junctional RyR2 Ca^{2+}flux (J^T_{ryr}) is given by,

$$J^T_{ryr} = \sum_{n=1}^{N} J^n_{ryr} \tag{S44}$$

The JSR luminal Ca2+ sensitivity formulation is given by,

$$\phi = \phi_b + \left(\frac{[Ca^{2+}]^n_{jsr}}{\phi_m}\right)^{\eta_\phi} \tag{S45}$$

where ϕ_b, ϕ_m, and η_ϕ are constants. The influence of ϕ on RyR2 $P_O$can be seen in Fig. S2.

Non-junctional RyR Ca^{2+} Channels

The Ca^{2+} flux from non-junctional or “rogue” RyR2s is

$$J_{ryr,nj} = \pi^o_{ryr,nj} v_{ryr,nj}([Ca^{2+}]_{nsr} - [Ca^{2+}]_i). \tag{S46}$$

where $v_{ryr,nj}$ is the total non-junctional RyR release rate in s^{-1} and $\pi^o_{ryr,nj}$ is the fraction of open non-junctional RyRs and solves

$$\frac{d\pi^o_{ryr,nj}}{dt} = \phi k^+ [Ca^{2+}]_i^{\eta_R}(1 - \pi^o_{ryr,nj}) - k^- \pi^o_{ryr,nj} \tag{S47}$$

where ϕ is the RyR2 luminal sensitivity function (see Eq. 1), k^+ and k^- are transition rates for a individual RyR as presented in Fig. 1B.

Slow Buffers

Slow buffers are lumped into the following flux,

$$J_{buffer} = \frac{dCaB_{trpn}}{dt} + \frac{dCaB_{calm}}{dt} + \frac{dCaB_{slm}}{dt} \tag{S48}$$

where $\frac{dCaB_{trpn}}{dt}$, $\frac{dCaB_{calm}}{dt}$, and $\frac{dCaB_{slm}}{dt}$ are ODEs governing the amount of Ca^{2+} bound to each buffer, given by,

$$\begin{aligned}
\frac{dCaB_{trpn}}{dt} &= k_{on,trpn}[Ca^{2+}]_i(B^T_{trpn} - CaB_{trpn}) - k_{off,trpn}CaB_{trpn} \\
\frac{dCaB_{calm}}{dt} &= k_{on,calm}[Ca^{2+}]_i(B^T_{calm} - CaB_{calm}) - k_{off,calm}CaB_{calm} \\
\frac{dCaB_{slm}}{dt} &= k_{on,slm}[Ca^{2+}]_i(B^T_{slm} - CaB_{slm}) - k_{off,slm}CaB_{slm}
\end{aligned}$$

Ca^{2+} Indicators

While not always used, the model is capable of simulation the flux of Ca^{2+} onto Ca^{2+} indicators (e.g., Fluo-4) given by,

$$J_{CaF} = \frac{d[CaF]}{dt} \tag{S49}$$

where $\frac{d[CaF]}{dt}$ governs the amount of Ca^{2+} bound to the indicator (F) and is given by,

$$\frac{d[CaF]}{dt} = -k_{off,F}[CaF] + k_{on,F}[Ca^{2+}]_i\left([F]^T - [CaF]\right) \tag{S50}$$

where $[F]^T$ is the total amount of fluorescent indicator in the cytosolic compartment (e.g., 50 μM) and $k_{on,F}$ and $k_{off,F}$ are the on and off rates for Ca^{2+} binding to the fluorescent indicator, respectively.

Nernst reversal potentials

$$E_{ca} = \frac{RT}{zF}\log\left(\frac{[Ca^{2+}]_o}{[Ca^{2+}]_i}\right) \tag{S51}$$

$$E_{na} = \frac{RT}{zF}\log\left(\frac{[Na^{+}]_o}{[Na^{+}]_i}\right) \tag{S52}$$

$$E_{k} = \frac{RT}{zF}\log\left(\frac{[K^{+}]_o}{[K^{+}]_i}\right) \tag{S53}$$

where z is the valency for the respective ion.

Dynamic Buffering Fractions

Myoplasmic Buffering

Buffering in the myoplasm is approximated using a dynamic buffering fraction given by

$$\beta_{myo} = \left(1 + \frac{B^T_{myo}K^{myo}_m}{(K^{myo}_m + [Ca^{2+}]_i)^2}\right)^{-1} \tag{S54}$$

where B^T_{myo} is the total myoplasmic buffer concentration, K^{myo}_m is the half saturation constant for the myoplasmic buffer.

Junctional SR Buffering

Buffering in each JSR compartment is approximated using a dynamic buffering fraction given by

$$\beta_{jsr}^{n} = \left(1 + \frac{B_{jsr}^{T} K_{m}^{jsr}}{(K_{m}^{jsr} + [Ca^{2+}]_{jsr}^{n})^{2}}\right)^{-1} \tag{S55}$$

where B_{jsr}^{T} is the total JSR buffer concentration, K_{m}^{jsr} is the half saturation constant for the JSR buffer.

Fast Subspace

Similar to previous work [7, 8, 6] this model formulation leads to a rapid equilibrium of the $[Ca^{2+}]_{ds}$ with the $[Ca^{2+}]_{i}$ and $[Ca^{2+}]_{jsr}$. Thus, in each dyadic subspace we assume a $[Ca^{2+}]$ ($[Ca^{2+}]_{ds,ss}^{n}$) that balances the fluxes in and out of that compartment,

$$0 = \frac{\beta_{ds}}{\lambda_{ds}} \left(J_{lcc}^{n} + J_{ryr}^{n} - J_{efflux}^{n}\right),$$

that is,

$$[Ca^{2+}]_{ds,ss}^{n} \approx \frac{N_{L,O}^{n}\, J_{lcc}^{0} + v_{efflux}[Ca^{2+}]_{i} + N_{R,O}^{n}\, v_{ryr}[Ca^{2+}]_{jsr}^{n}}{N_{R,O}^{n}\, v_{ryr} + v_{efflux} - N_{L,O}^{n}\, J_{lcc}^{1}}. \tag{S56}$$

3D Spatial Model

The model describes a single sarcomere (M-line to M-line) centered on a Z-line that contains numerous equally distributed CRUs. The model geometry is $4 \times 4 \times 14$ μm with CRUs centered in space and, consistent with experimental findings, separated from one another by 600 nm [61]. The spatial-temporal evolution of [Ca2+]i and the Ca2+-bound Fluo4 concentration ([CaF]) were simulated using PDEs for $[Ca^{2+}]_{i}$ diffusion and the diffusion of Ca^{2+}-bound indicator ([CaF], i.e., Fluo-4). These reaction-diffusion style equations are as follows,

$$\frac{\delta[Ca^{2+}]_{i}}{\delta t}\left(\frac{1}{\beta_{i}}\right) = D_{Cai}\nabla^{2}[Ca^{2+}]_{i} + (\lambda_{dsi}J_{efflux} - J_{serca} - J_{ncx} + J_{bca} - J_{buffer} - J_{CaF}) \tag{S57}$$

$$\frac{\delta[CaF]}{\delta t} = D_{CaF}\nabla^{2}[CaF] + J_{CaF} \tag{S58}$$

where λ_{dsi} is the volume fraction for subspace to cytosol, β_{i} is the cytosolic dynamic buffering fraction, and the cytosolic fluxes (e.g., $J_{efflux}, J_{serca}, J_{ncx}, J_{bca}, J_{buffer}, \text{and} J_{CaF}$) retain similar formulations to corresponding fluxes in the compartment model (see above). The PDEs are numerically integrated using a centered difference in space and forward Euler in time solver and the ODEs for $[Ca^{2+}]_{ds}$ and $[Ca^{2+}]_{jsr}$ remain unchanged. Linescan images were generated by assessing [CaF] over time after simulated optical blurring and with the addition of Gaussian noise, as previously described in Smith et al. [62].

Tables of Model Parameters

Table S1: Model Geometry

Parameter	Definition	Value
V_{cell}	Cell volume	36 pL
V_{myo}	Myoplasmic volume	18 pL
V_{nsr}	NSR volume	1.152 pL
V_{jsr}	JSR volume	0.18 pL
V_{ds}	Subspace volume	54 nL
λ_{nsr}	NSR volume fraction	0.064
λ_{jsr}	JSR volume fraction	0.01
λ_{ds}	Subspace volume fraction	0.003

Table S2: RyR2 Ca^{2+} Channel Parameters

Parameter	Definition	Value
N_R	number of RyR2s per CRU	50
k^+	RyR Ca^{2+} association rate constant	0.2 $\mu M^{-\eta_R}$ s^{-1}
k^-	RyR Ca^{2+} disassociation rate constant	425 s^{-1}
η_R	Ca^{2+}-binding cooperativity factor	2.2
ϕ_m	Luminal Ca^{2+} regulation coefficient	0.8025 mM
ϕ_b	Luminal Ca^{2+} regulation coefficient	1500
η_ϕ	Luminal Ca^{2+} regulation coefficient	4
v_{ryr}^T	Total junctional RyR2 release rate	48
v_{ryr}	single RyR2 release rate	$v_{ryr}/(N \times N_R)$
$v_{ryr,nj}$	Total non-junctional RyR2 release rate	9.6

Table S3: L-type Ca^{2+} Channel Parameters

Parameter	Definition	Value
N_L	Number of LCCs per CRU	6
M_L	Number of states per LCC	7
η_L	Ca^{2+} cooperativity parameter	2
k_{25}	C_2 to A_5 rate constant	450 s^{-1}
k_{16}	R_1 to R_6 rate constant	450 s^{-1}
k_{34}	I_3 to I_4 rate constant	450 s^{-1}
k_{21}	C_2 to R_1 rate constant	31.5 s^{-1}
k_{76}	O_7 to R_6 rate constant	31.5 s^{-1}
k_{23}	C_2 to I_3 rate constant	$0.5\mu M^{-\eta_L}$ s^{-1}
k_{74}	O_7 to I_4 rate constant	$0.5\mu M^{-\eta_L}$ s^{-1}
k_{12}	R_1 to C_2 rate constant	2 s^{-1}
k_{32}	I_3 to C_2 rate constant	2 s^{-1}
k_{75}	O_7 to A_5 rate constant	1800 s^{-1}
k_{61}	R_6 to R_1 rate constant	500 s^{-1}
k_{52}	A_5 to C_2 rate constant	500 s^{-1}
k_{43}	I_4 to I_3 rate constant	500 s^{-1}
k_{57}	A_5 to O_7 rate constant	400 s^{-1}
k_{67}	R_6 to O_7 rate constant	0.4444 s^{-1}
k_{47}	R_4 to O_7 rate constant	0.4444 s^{-1}
$V_{\sigma,1}$	VDA parameter	6
$V_{\theta,1}$	VDA parameter	2
$V_{\sigma,3}$	VDD parameter	2
$V_{\theta,3}$	VDD parameter	-50
P_{lcc}^T	Total junctional LCC permeability to Ca^{2+}	0.0002375
P_{lcc}	single junctional LCC permeability to Ca^{2+}	$P_{lcc}^T/(N \times N_L)$
$P_{lcc,nj}$	Total non-junctional LCC permeability to Ca^{2+}	0.000475

Table S4: K^+ current Parameters

Parameter	Definition	Value
g_{ktof}	Maximum I_{ktof} conductance	0.45 mS μF^{-1}
g_{ktos}	Maximum I_{ktos} conductance	0.135 mS μF^{-1}
g_{kss}	Maximum I_{kss} conductance	0.0405 mS μF^{-1}
g_{k1}	Maximum I_{k1} conductance	0.2 mS μF^{-1}
g_{bk}	Maximum I_{bk} conductance	0.0082 mS μF^{-1}

Table S5: Na^+ current Parameters

Parameter	Definition	Value
g_{na}	Maximum I_{na} conductance	10 mS μF^{-1}
g_{bna}	Maximum I_{bna} conductance	0.0016 mS μF^{-1}

Table S6: Pump and Exchanger Parameters

Parameter	Definition	Value
I_{pmca}^{max}	Maximal PMCA current	0.1875 pA pF^{-1}
K_{pmca}	Ca^{2+} half saturation constant for PMCA	0.25 μM
I_{ncx}^{max}	Maximal NCX current	750 pA pF^{-1}
η_{ncx}	NCX voltage dependence coefficient	0.35
$K_{ncx,ca}$	Ca^{2+} half saturation contant for NCX	1380 μM
$K_{ncx,na}$	Na^{+} half saturation contant for NCX	87500 μM
k_{ncx}^{sat}	NCX exchange saturation factor	0.1
$K_{ma,ncx}$	NCX allosteric activation constant	0.150 μM
A_p	Concentration of SERCA molecules	150 μM
I_{nak}^{max}	Maximal I_{nak} current	1.408 pA pF^{-1}
$K_{m,nai}$	half saturation for NaK	21000 μM
$K_{m,ko}$	half saturation for NaK	1500 μM

Table S7: Buffering Parameters

Parameter	Definition	Value
β_{ds}	Subspace Ca^{2+} buffering fraction	0.1
β_{nsr}	NSR Ca^{2+} buffering fraction	1
B_{myo}^{T}	Total myoplasmic Ca^{2+} buffer concentration	132 μM
K_{m}^{myo}	Half saturation constant for myoplasmic Ca^{2+} buffer	0.6 μM
B_{jsr}^{T}	Total JSR Ca^{2+} buffer concentration	140 $\times$ 30 mM
K_{m}^{jsr}	Half saturation constant for JSR Ca^{2+} buffer	638μM
B_{trpn}^{T}	Total troponin buffer concentration	140
k_{trpn}^{on}	Slow troponin buffer on rate	2.37 s^{-1}
k_{trpn}^{off}	Slow troponin buffer off rate	0.032 s^{-1}
B_{calm}^{T}	Total calmodulin buffer concentration	24
k_{calm}^{on}	Slow calmodulin buffer on rate	34 s^{-1}
k_{calm}^{off}	Slow calmodulin buffer off rate	238 s^{-1}
B_{slm}^{T}	Total sarcolemmal membrane buffer concentration	42
k_{slm}^{on}	Slow sarcolemmal membrane buffer on rate	100 s^{-1}
k_{slm}^{off}	Slow sarcolemmal membrane buffer off rate	1300 s^{-1}
F_{4}^{T}	Total Fluo-4 concentration	50 μM
k_{F4}^{on}	Slow sarcolemmal membrane buffer on rate	100 s^{-1}
k_{F4}^{off}	Slow sarcolemmal membrane buffer off rate	110 s^{-1}
F_{5N}^{T}	Total Fluo-5N concentration	0 (or 50 if specified) μM
k_{F5N}^{on}	Slow sarcolemmal membrane buffer on rate	80 s^{-1}
k_{F5N}^{off}	Slow sarcolemmal membrane buffer off rate	32,000 s^{-1}

Table S8: Initial Conditions

Parameter	Definition	Value
V	Membrane voltage	-81 mV
$[Na^+]_i$	Myoplasmic [Na^+]	10.2 mM
$[K^+]_i$	Myoplasmic [K^+]	143.72 mM
$[Ca^{2+}]_i$	Myoplasmic [Ca^{2+}]	80 nM
$[Ca^{2+}]_o$	Extracellular [Ca^{2+}]	1.8 mM
$[Ca^{2+}]_{ds}$	Dyadic subspace [Ca^{2+}]	80 nM
$[Ca^{2+}]_{nsr}$	Network SR [Ca^{2+}]	900 mM
$[Ca^{2+}]_{jsr}$	Junctional SR [Ca^{2+}]	900 mM
m_{na}	I_{na} activation gate variable	0.0015
h_{na}	I_{na} inactivation gate variable	0.9849
j_{na}	I_{na} inactivation gate variable	0.9905
a_{ktof}	I_{ktof} activation gating variable	0.0021
i_{ktof}	I_{ktof} inactivation gate variable	1
a_{ktos}	I_{ktos} activation gate variable	2.9871e-04
i_{ktos}	I_{ktos} inactivation gate variable	0.9994
a_{kss}	I_{kss} activation gate variable	0.002
i_{kss}	I_{kss} inactivation gate variable	1
$\pi^o_{ryr,nj}$	fraction of open non-junctional RyR2s	0
$\pi^o_{lcc,nj}$	fraction of open non-junctional LCCs	0

Table S9: Other Parameters

Parameter	Definition	Value
F	Faraday constant	9.6485×10^4 coul mol^{-1}
T	Temperature	310 K
R	Ideal gas constant	8314 J $mmol^{-1}$ K^{-1}
g_{bca}	Maximal backgroung Ca^{2+} conductance	1.1024×10^{-4} mS μF
v^T_{refill}	Total JSR refill rate	2.5 s^{-1}
v^T_{efflux}	Total rate of Ca^{2+} efflux out of the susbspace	200 s^{-1}
A_m	Capacitative area of cell membrane	1.5340×10^{-4} μF
z	Valency for Ca^{2+}	2

Supporting Material Figures

Steady-state RyR2 Open Probability

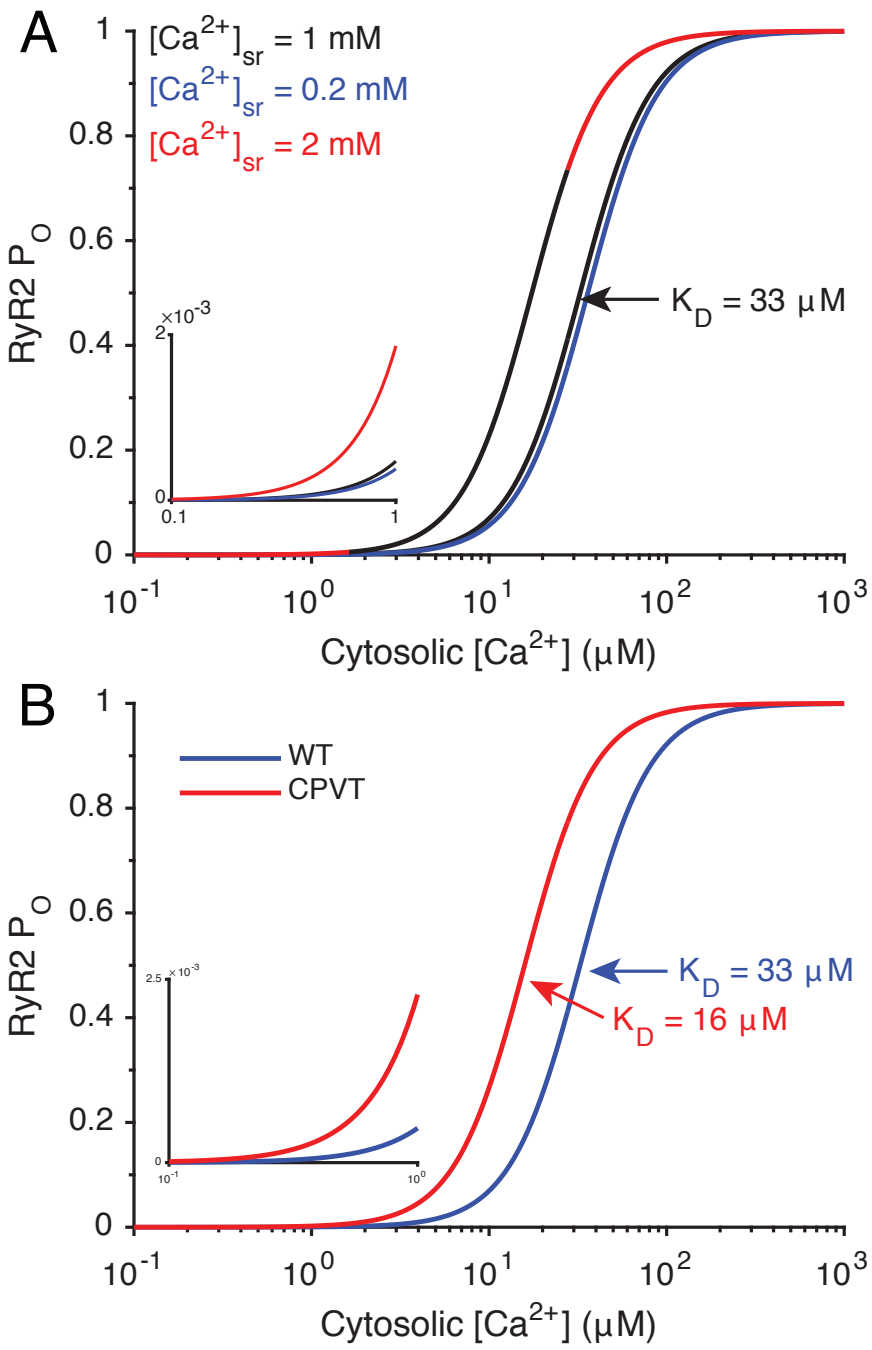

Figure S1: Steady-state RyR2 open probability (P_O) as function of $[Ca^{2+}]_i$. A) RyR2 P_O for 3 different $[Ca^{2+}]_{sr}$ levels B) RyR2 P_O for WT and CPVT conditions.

EC Coupling Gain & Gradedness

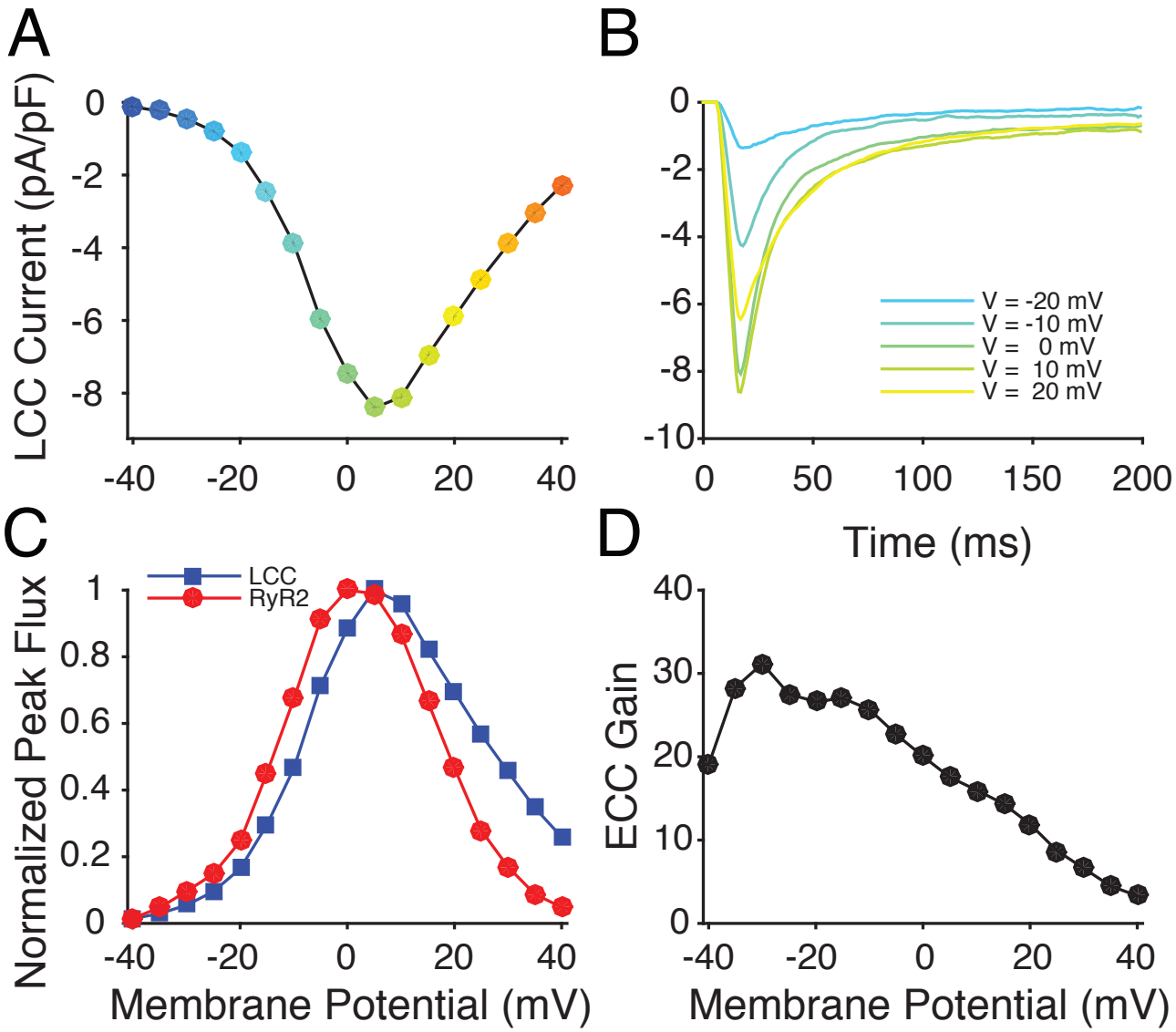

Figure S2: EC Coupling Dynamics. A) Peak LCC current from the novel 7-state LCC (see Fig. 1B) as a function of membrane potential. B) Representative LCC currents for various holding potentials. C) Normalized peak LCC (blue line) and RyR2 (red line) fluxes as function of membrane potential D) ECC gain as defined as peak of J^T_{ryr}/J^T_{lcc}.

Quiescent Ca^{2+} spark dynamics

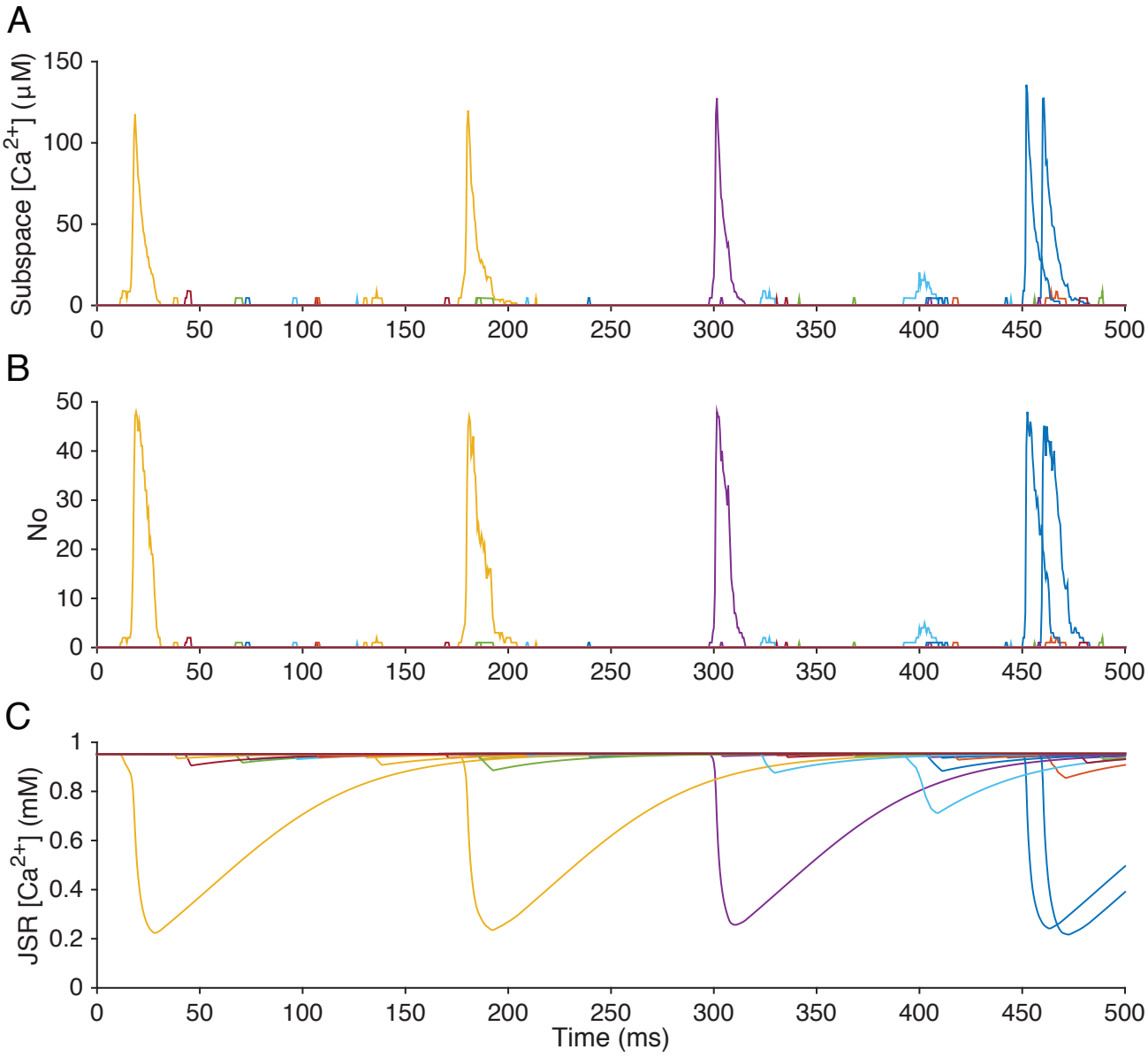

Figure S3: Ca^{2+} Sparks and SR Ca^{2+} leak under quiescent, **normal** conditions. Time evolution of A) $[Ca^{2+}]_{ds}$ B) $N^{n}_{R,O}$, and C) $[Ca^{2+}]_{jsr}$ during a 500 ms simulation of a quiescent cardiomyocyte. Each color represents the behavior from a different CRU within the whole-cell model. For clarity only 10% of the cell's 20,000 CRUs are shown.

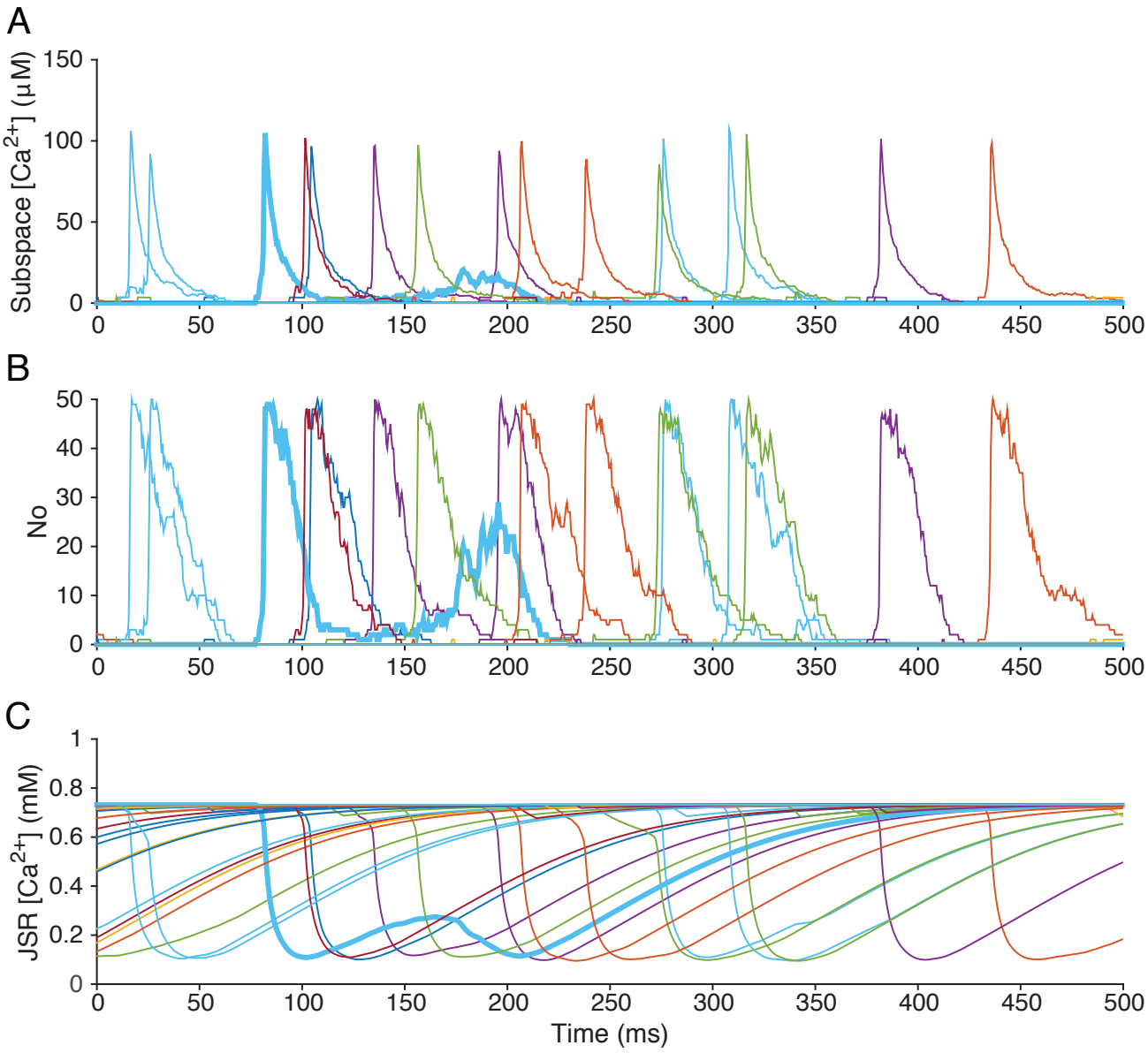

Figure S4: Ca^{2+} Sparks and SR Ca^{2+} leak under quiescent, **leaky RyR2** conditions. Time evolution of A) $[Ca^{2+}]_{ds}$ B) $N^{n}_{R,O}$, and C) $[Ca^{2+}]_{jsr}$ during a 500 ms simulation of a quiescent cardiomyocyte. Each color represents the behavior from a different CRU within the whole-cell model. For clarity only 10% of the cell's 20,000 CRUs are shown.

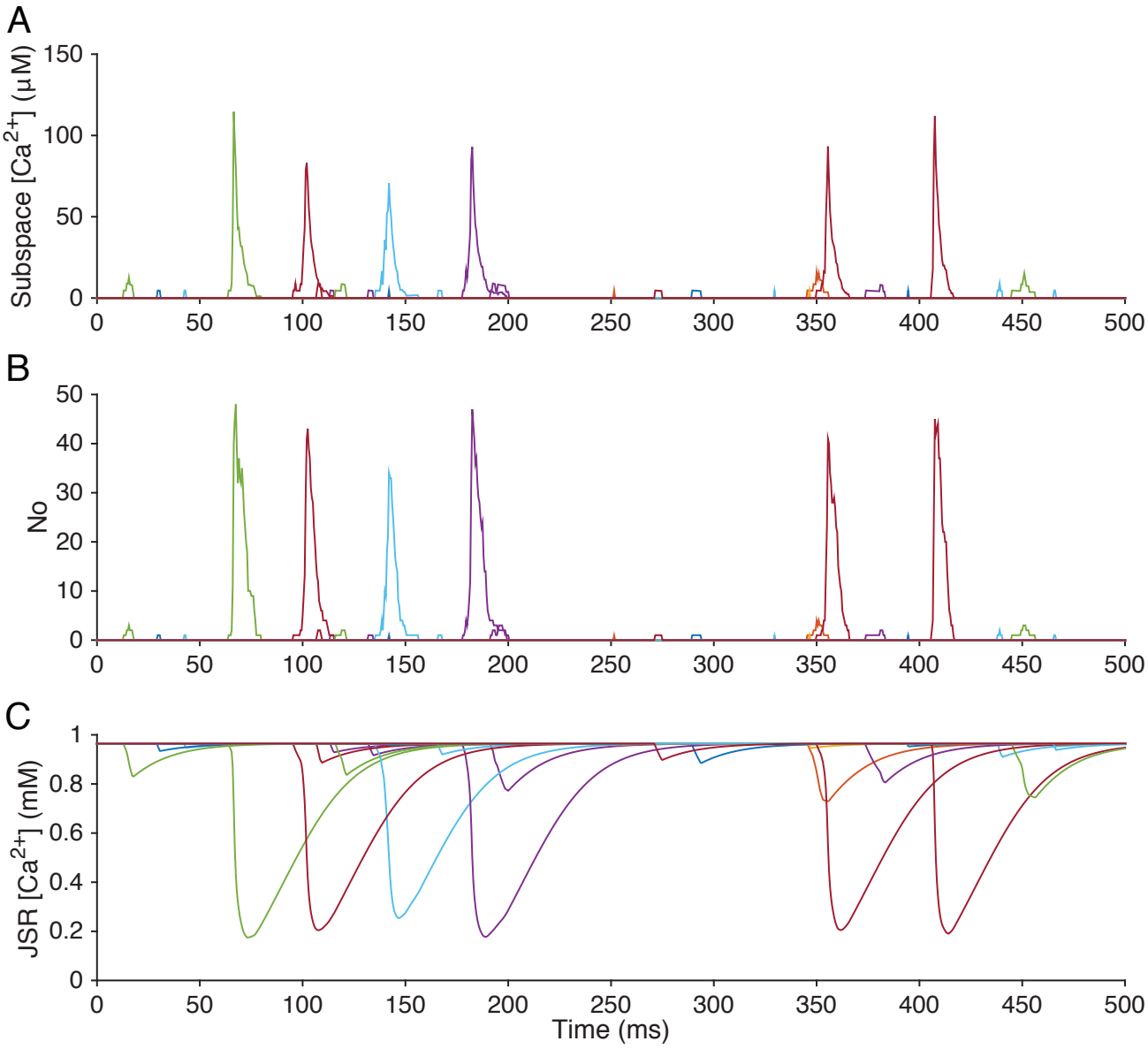

Figure S5: Ca^{2+} Sparks and SR Ca^{2+} leak under quiescent, **decreased JSR buffering** conditions. Time evolution of A) $[Ca^{2+}]_{ds}$ B) $N^{n}_{R,O}$, and C) $[Ca^{2+}]_{jsr}$ during a 500 ms simulation of a quiescent cardiomyocyte. Each color represents the behavior from a different CRU within the whole-cell model. For clarity only 10% of the cell's 20,000 CRUs are shown.

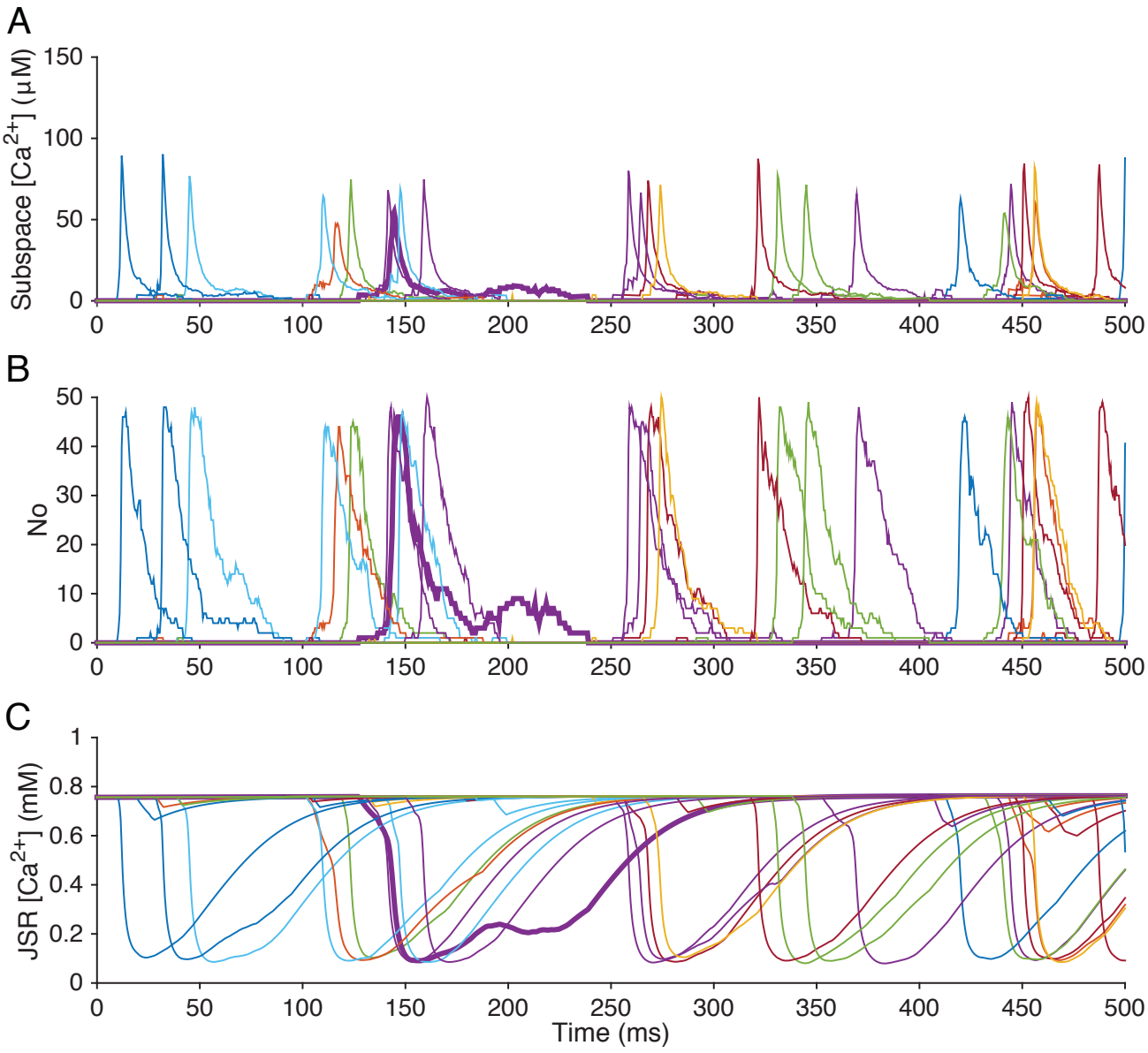

Figure S6: Ca^{2+} Sparks and SR Ca^{2+} leak under quiescent, **CPVT** (i.e., leaky RyR2 and decreased JSR buffering) conditions. Time evolution of A) $[Ca^{2+}]_{ds}$ B) $N^{n}_{R,O}$, and C) $[Ca^{2+}]_{jsr}$ during a 500 ms simulation of a quiescent cardiomyocyte. Each color represents the behavior from a different CRU within the whole-cell model. For clarity only 10% of the cell's 20,000 CRUs are shown.

Membrane currents

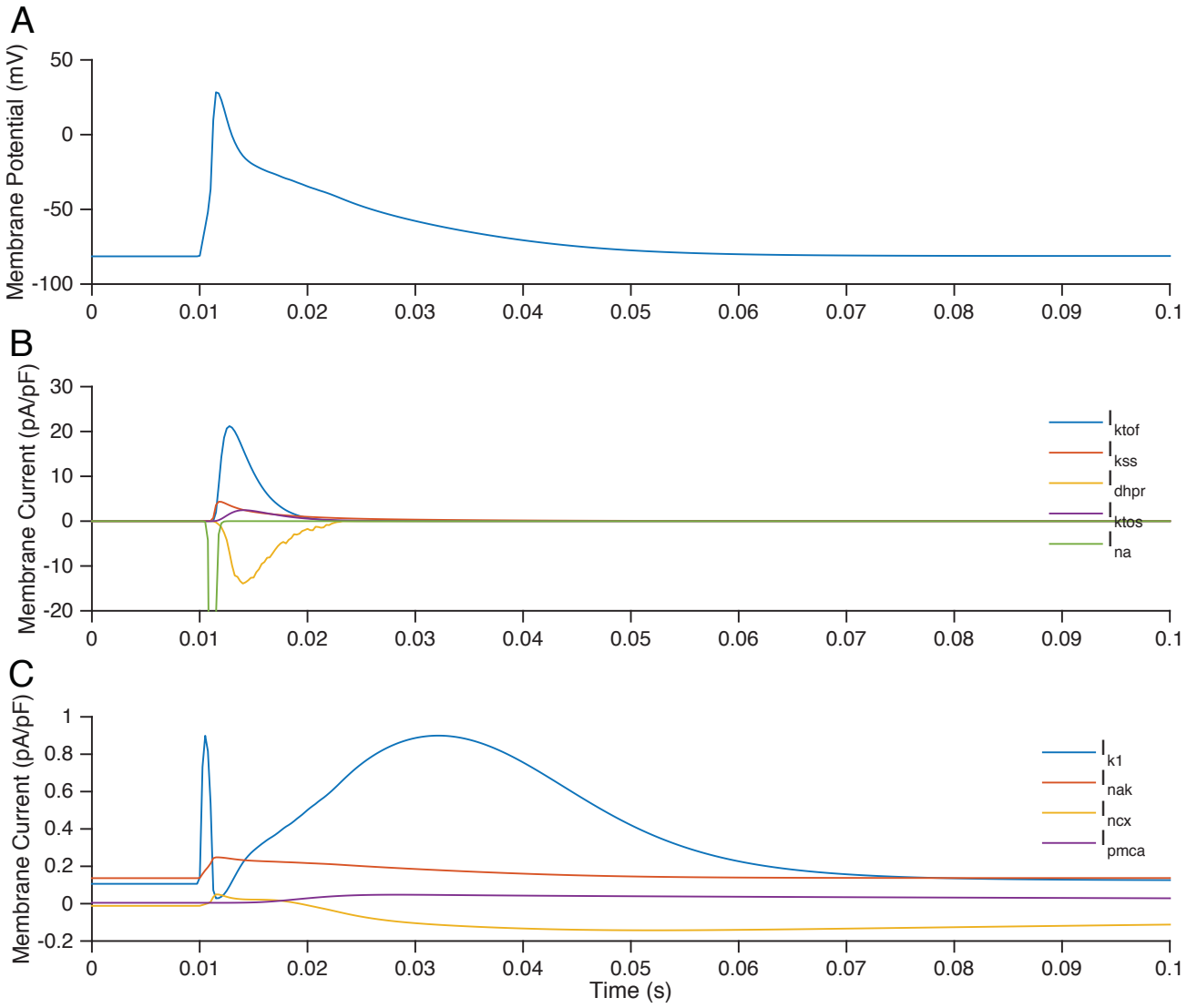

Figure S7: Membrane potential and key sarcolemmal currents during AP.

Systolic Ca^{2+} release dynamics

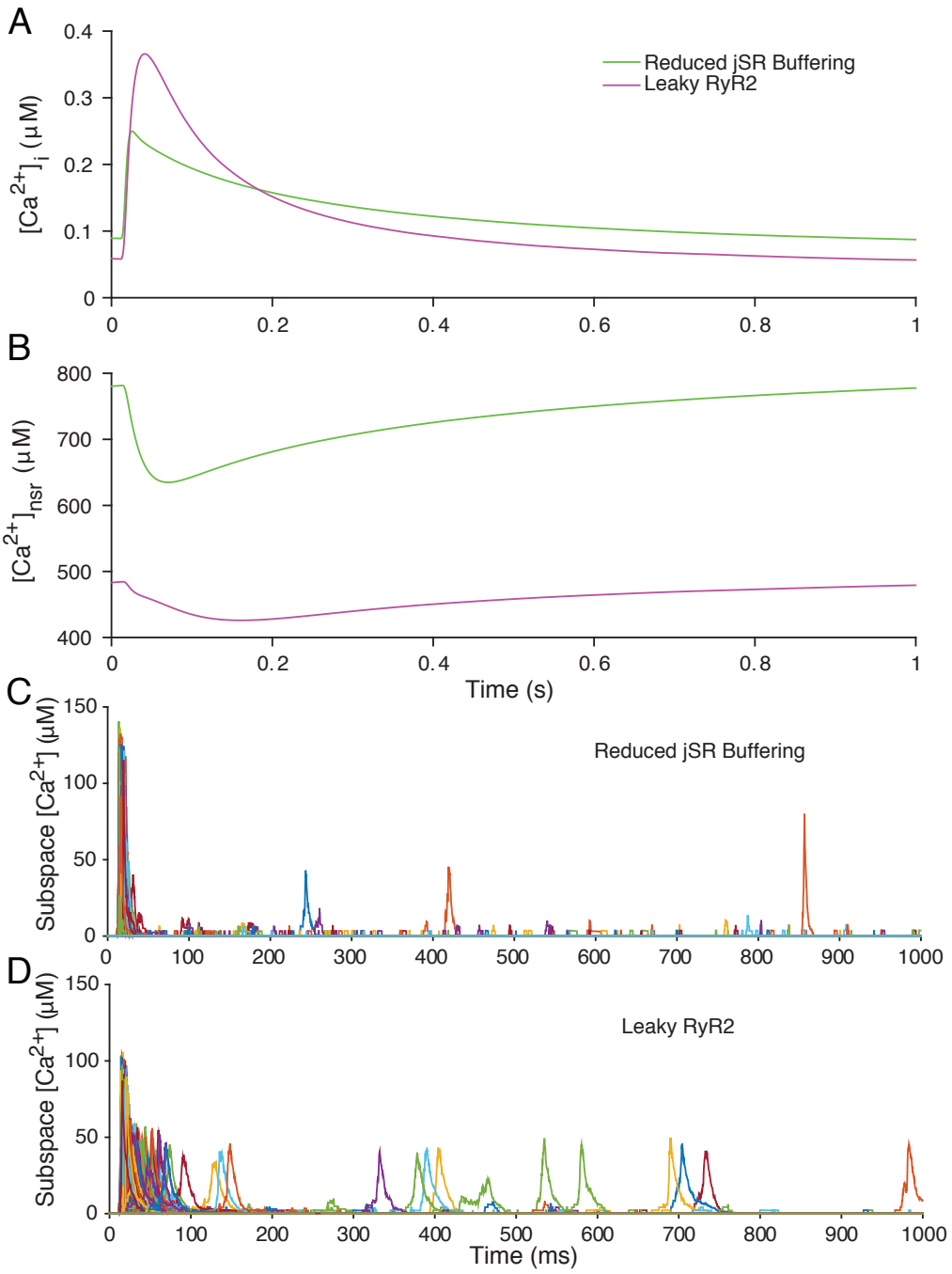

Figure S8: Systolic Ca^{2+} release dynamics with reduced JSR buffering and leaky RyR2s. A) Bulk $[Ca^{2+}]_i$ B) Bulk $[Ca^{2+}]_{sr}$ C) Ca^{2+} sparks with reduced JSR buffering, and D) Ca^{2+} sparks during leaky RyR2 conditions.

WT spatial Ca^{2+} release dynamics

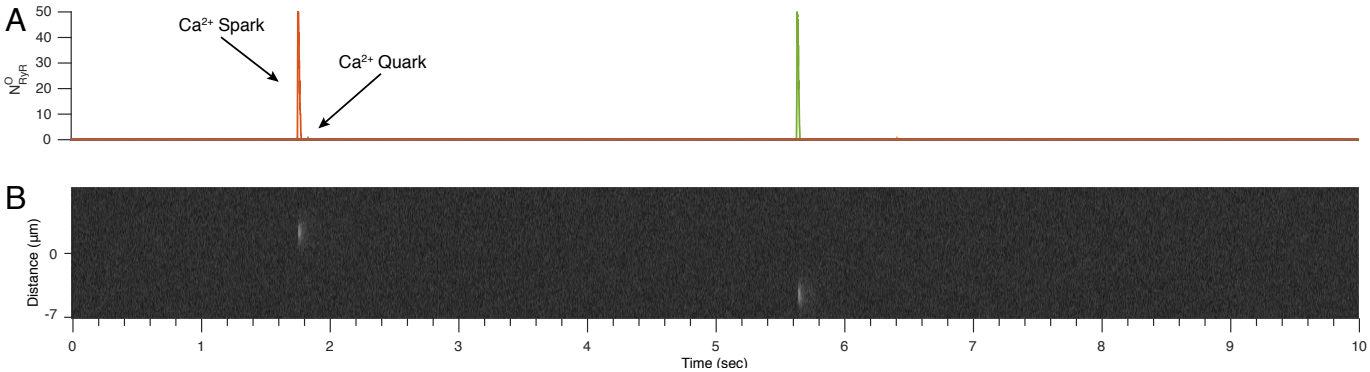

Figure S9: Ca^{2+} release behavior during WT . A) Stochastic RyR2 gating during quiescent, WT conditions and B) simulated transverse line-scan of quiescent Ca^{2+} release dynamics (as F/F_o) during WT conditions. Realistic noise and confocal blurring are added after simulation. Optical blurring was perfomed using a model point spread function (PSF) consistent with confocal PSFs (i.e., 400 nm in the x,y direction and 800 nm in the z direction). White noise equalling 10% of F/F_o was added after optical blurring.

$[Ca^{2+}]_i$ dynamics during rapid pacing

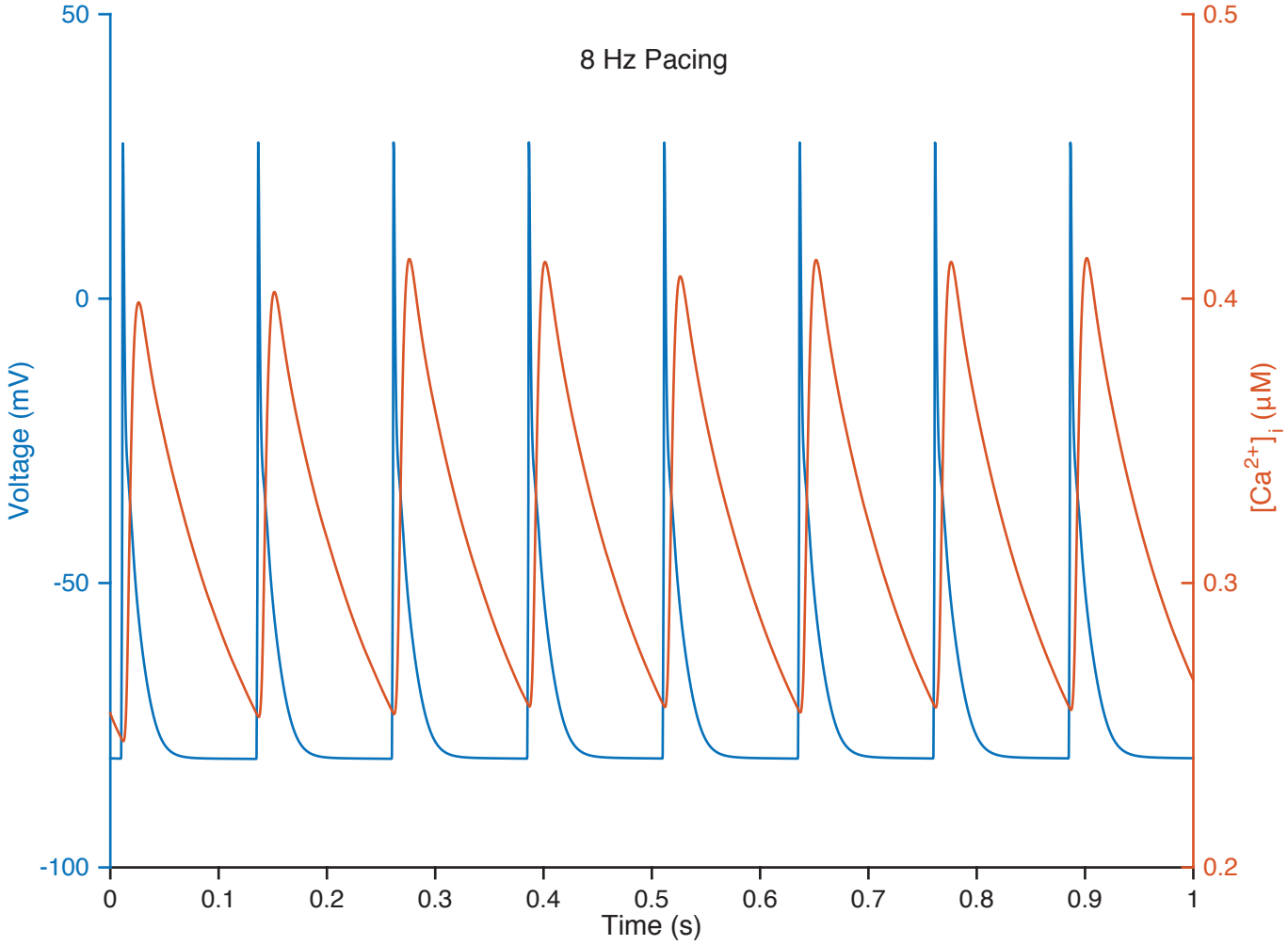

Figure S10: Action potentials (left axis, blue line) and $[Ca^{2+}]_i$ transients (right axis, red lines) generated by the model at 8 Hz.

$[Ca^{2+}]_i$ dynamics during perforated-patch APs and Rabbit APs

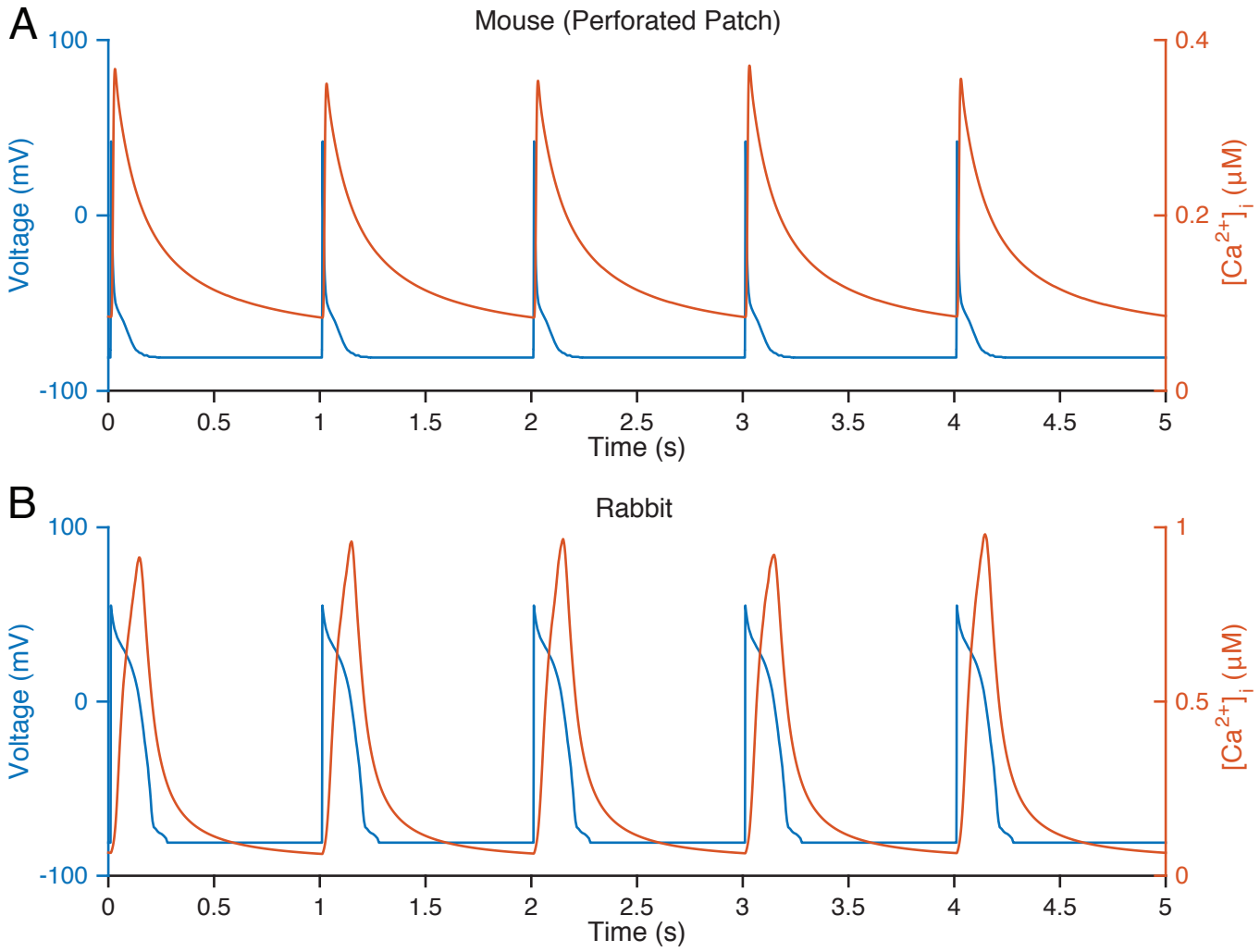

Figure S11: A) $[Ca^{2+}]_i$ transients (right axis, red lines) generated by the model when membrane potential (V) is clamped to an experimental, perforated-patch, mouse AP (left axis, blue line) (digitized from [3]). B) $[Ca^{2+}]_i$ transients (right axis, red lines) generated by the model when membrane potential (V) is clamped to an experimental, ruptured-patch, rabbit AP (left axis, blue line) (digitized from [4])

References

[1] Vladimir E Bondarenko, Gyula P Szigeti, Glenna C L Bett, Song-Jung Kim, and Randall L Rasmusson. Computer model of action potential of mouse ventricular myocytes. *American journal of physiology Heart and circulatory physiology*, 287(3):H1378–403, September 2004.

[2] Jeffrey J Fox, Jennifer L McHarg, and Robert F Gilmour. Ionic mechanism of electrical alternans. *American journal of physiology Heart and circulatory physiology*, 282(2):H516–30, February 2002.

[3] R Macianskiene, V Bito, L Raeymaekers, B Brandts, K R Sipido, and K Mubagwa. Action potential changes associated with a slowed inactivation of cardiac voltage-gated sodium channels by KB130015. *British journal of pharmacology*, 139(8):1469–1479, August 2003.

[4] J L Puglisi, W Yuan, J W Bassani, and D M Bers. Ca^{2+} influx through Ca^{2+} channels in rabbit ventricular myocytes during action potential clamp: influence of temperature. *Circulation research*, 85(6):e7–e16, September 1999.

[5] Kenneth Tran, Nicolas P Smith, Denis S Loiselle, and Edmund J Crampin. A thermodynamic model of the cardiac sarcoplasmic/endoplasmic Ca(2+) (SERCA) pump. *Biophysical journal*, 96(5):2029–2042, March 2009.

[6] George S B Williams, Aristide C Chikando, Hoang-Trong M Tuan, Eric A Sobie, W J Lederer, and M Saleet Jafri. Dynamics of Calcium Sparks and Calcium Leak in the Heart. *Biophysical journal*, 101(6):1287–1296, September 2011.

[7] George S B Williams, Marco A Huertas, Eric A Sobie, M Saleet Jafri, and Gregory D Smith. A probability density approach to modeling local control of calcium-induced calcium release in cardiac myocytes. *Biophysical journal*, 92(7):2311–2328, January 2007.

[8] George S B Williams, Marco A Huertas, Eric A Sobie, M Saleet Jafri, and Gregory D Smith. Moment closure for local control models of calcium-induced calcium release in cardiac myocytes. *Biophysical journal*, 95(4):1689–1703, August 2008.